Energy Storage

WILEY

ENERGY STORAGE

RESEARCH ARTICLE

Comparative Computational Study of Semi-Metallic Zintl Hydrides for Hydrogen Storage Applications

H. Ammi[1] | Z. Charifi[2,3] | T. Ghellab[2,3] | T. Saadi[2,3] | L. Bouhdjer[1] | S. Addala[1] | H. Baaziz[2,3]

[1]Department of Physics, Faculty of Exact Sciences, Laboratory of Material Physics and Optoelectronic Compounds, University of Bouira, Bouira, Algeria | [2]Department of Physics, Faculty of Science, University of M'sila, M'sila, Algeria | [3]Laboratory of Physics and Chemistry of Materials, University of M'sila, M'sila, Algeria

Correspondence: H. Baaziz (hakim.baaziz@univ-msila.dz; baaziz_hakim@yahoo.fr)

Received: 4 June 2025 | **Revised:** 21 September 2025 | **Accepted:** 13 October 2025

Funding: The authors received no specific funding for this work.

Keywords: electronic and mechanical properties | gravimetric hydrogen capacity | hydrogen desorption temperature | hydrogen storage | Zintl phase hydrides

ABSTRACT

Efficient, safe, and compact solid-state materials are critical for overcoming hydrogen storage challenges. This study introduces a novel class of materials, the hexagonal Zintl-phase hydrides SnMSiH (M = Al, Ga), and establishes their exceptional potential through first-principles density functional theory (DFT) calculations. The key superiority of these materials lies in their unique semimetallic electronic structure, which significantly enhances hydrogen interactions by reducing the activation energy for desorption, enabling efficient and reversible cycling—a critical improvement over insulating or wide-bandgap hydrides. Structurally, the primitive hexagonal framework (space group P3m1) provides optimal diffusion pathways for hydrogen. We report a high gravimetric capacity of 0.58 wt% for SnAlSiH with a near-ambient desorption temperature of 310.69 K, markedly superior to many complex hydrides. SnGaSiH offers a capacity of 0.47 wt% at an even lower desorption temperature of 254.15 K, indicating easy hydrogen release. Thermodynamically, both compounds exhibit significant thermal expansion and high heat capacities, ensuring resilience at operating temperatures. Mechanically, they are highly anisotropic; SnAlSiH's higher compressibility may facilitate volume changes during cycling, while SnGaSiH demonstrates superior mechanical stability (higher elastic constants). This combination of favorable desorption thermodynamics, intrinsic structural stability, and robust mechanical properties distinguishes SnMSiH hydrides as premier candidates for application. This work provides a foundational strategy for further performance enhancement through alloying and defect engineering.

1 | Introduction

Energy generation has been a fundamental aspect of human civilization for centuries. However, the increasing reliance on fossil fuels has led to environmental concerns and the depletion of hydrocarbon resources. Several alternative energy sources have been explored to mitigate greenhouse gas emissions and reduce dependence on fossil fuels [1, 2]. The global pursuit of sustainable energy is driven by multiple factors, including political pressures from energy-importing nations, environmental concerns linked to the Kyoto Protocol, and the declining availability of petroleum reserves [3]. As a response to these challenges, hydrogen-based energy has emerged as a promising solution [4]. Unlike hydrocarbons,

hydrogen combustion does not release carbon into the environment, and advancements in hydrogen-related technologies are making its production and utilization more cost-effective over time.

With global petroleum supplies projected to be exhausted in approximately 41 years and energy consumption expected to increase by 56% by 2040 [5], the need for clean and efficient energy sources has become more urgent. Renewable energy alternatives such as hydropower, wind, solar, bioenergy, tidal, and hydrogen energy are actively being developed [6]. Petroleum stocks and other non-renewable energy sources will eventually run out. Therefore, it is necessary to identify, develop, and guarantee the sustainability of new energy supplies. Because of its availability and advantages for the environment, hydrogen in particular is receiving [7, 8]. By 2050, global hydrogen demand is expected to rise by 700% [9, 10]. To meet this growing demand, researchers are exploring materials with high hydrogen concentrations that function efficiently at low operating temperatures.

Hydrogen storage in high-pressure tanks remains a viable solution; however, it is accompanied by efficiency losses due to compression, potential safety risks, and significant infrastructure demands. Consequently, research has pivoted toward solid-state hydrogen storage, which offers superior energy densities in both gravimetric and volumetric terms [11, 12]. Among these alternatives, metal hydrides and complex hydrides stand out for their ability to reversibly adsorb and desorb hydrogen through chemical reactions [11].

Zintl phases have emerged as promising materials in hydrogen storage research. These compounds, first described by Eduard Zintl, consist of electropositive metals paired with group 13–15 elements, forming semiconducting structures with a unique blend of covalent and ionic bonding. Their electronic structure and composition make them attractive for energy storage applications, as they enable controlled hydrogen uptake and release under favorable conditions.

Zintl's electron counting principles aid in predicting structural formations and elucidating structure–property correlations [13, 14]. Recent research on Zintl phase-derived polar semiconductors has revealed their potential for hydrogen storage, optoelectronics, and solar energy applications. AeTrTt materials, where Ae represents Ca, Sr., or Ba, Tr corresponds to Al or Ga, and Tt includes Si, Ge, or Sn.exhibit bandgaps between 0.3 and 0.8 eV upon hydrogenation [15–17].

Experimentally verified compounds such as $SrAl_2H_2$ and $BaGa_2H_2$ in the AB_2H_2 series have demonstrated promising hydrogen storage capabilities and structural integrity. However, $BaAl_2H_2$ remains challenging to synthesize on an industrial scale [18, 19]. Theoretical models suggest that these compounds adopt a hexagonal P3m1 structure, where hydrogen occupies interstitial sites and B atoms form graphite-like layers coordinated by three A-site atoms. This structural arrangement aligns with trends observed across similar Zintl-phase hydrides, offering predictability in designing new variants.

Understanding bonding interactions within these materials is crucial. While traditional Zintl frameworks propose formal charge separation (e.g., $(Ae)^{2+}[TrTtH]^{2-}$ or $[AeTrTt]^{1+}(H^-)$), modern band structure calculations indicate that hydrogen orbitals contribute primarily at energies 5 eV below the Fermi level, with limited hybridization near it [19–21]. This suggests a complex interplay between localized anionic models and nonlocal electronic activity, highlighting the need for further investigation.

This study employs computational methods to establish correlations between electronic, mechanical, and thermodynamic properties and their hydrogen storage performance. By bridging theoretical models with practical applications, we aim to develop design principles for next-generation hydrogen storage materials. The previous study performed making use of the Density Functional Theory (DFT) on the mechanical and thermal properties of the XAlSiH (X = Sr., Ca, Ba) hydrides. These are semiconductors having a band gap between 0.2 eV and 1.2 eV. Further, the hydrogen storage capabilities vary from 0.52% to 1.05% [22]. The Grüneisen parameter, heat capacity, and thermal expansion coefficient will also be studied, which will give information about their application in electronic and hydrogen storage.

In contrast, our investigations into XGaSiH hydrides (X = Sr., Ca, Ba) using the Full-Potential Linearized Augmented Plane Wave (FP-LAPW) approach in WIEN2k revealed hydrogen storage capacities between 0.34% and 0.47%, with bandgaps ranging from 0.1 to 1.0 eV. These findings indicate that performance improvements could be achieved through doping or structural modifications, making these materials viable candidates for renewable energy applications [23].

This study employs density functional theory (DFT) to investigate the structural, electronic, mechanical, and thermodynamic properties of SnMSiH (M = Al, Ga) Zintl phases, assessing their potential as solid-state hydrogen storage materials. The research is motivated by the need for safe and efficient alternatives to conventional high-pressure and cryogenic storage methods, which pose significant efficiency and cost challenges. Metal hydrides represent a promising solution due to their ability to reversibly absorb and desorb hydrogen under moderate operational conditions. Our comprehensive computational approach evaluates key performance metrics, including gravimetric hydrogen storage capacity, theoretical desorption temperatures, and entropy changes. Furthermore, we employ the Debye model to derive thermal properties such as heat capacity and the coefficient of thermal expansion, which are critical for understanding adsorption/desorption kinetics and material durability under thermal cycling. Mechanical stability is rigorously confirmed through calculations of elastic constants and moduli (e.g., bulk, shear, Young's), ensuring the compounds' resilience for practical applications.

The ultimate objective of this work is to establish fundamental structure–property relationships in these semi-metallic Zintl hydrides. By linking their electronic structure and mechanical behavior to hydrogen storage thermodynamics, this study provides a holistic foundation for the development of advanced, high-performance materials for sustainable energy storage.

2 | Details of Computation

The WIEN2k [24] package was used to model materials using the Full-Potential Linearized Augmented Plane Wave (FP-LAPW). The calculations used the local-density approximation (LDA) and the generalized-gradient approximation (GGA) [25] to incorporate exchange and correlation effects.

Intergrid region enhancement was achieved by extending the wavefunction by means of plane waves. Both SnAlSiH and SnGaSiH have been taken with $k_{max} \times R.M.T = 5.0$ as a cut-off for these plane waves in which R.M.T is a muffin tin sphere radius. To achieve $G_{max} = 16$ $(Ryd)^{1/2}$, the charge density was enhanced by the Fourier series. The muffin tin sphere was extended to $l_{max} = 10$ inside the valence wave function. The calculated energy gap between core and valence states was kept at −6.0 Ry. The self-consistent total energy threshold of 10^{-4}Ry guaranteed the convergence. To perform the sampling of the Brillouin zone, (B. Z) k-points are used as 600 k-points for SnAlSiH and 800 k-points for SnGaSiH. Because d or f orbitals are not partially filled, we did not use the Hubbard correction (GGA + U), which would give important bonding interactions at the experimental level. This study utilized a DFT-based approach at zero temperature and pressure and the term (PV) for considering pressure effects. We considered thermal effects by taking into account the vibrational contributions of the crystal free energy, which is important for further optimization of the production of the materials and prediction of their behavior in different conditions. The Gibbs2 code, created by Blanco et al. [26, 27], was used to calculate extensive thermodynamic properties within the quasi-harmonic Debye framework [28], including temperature-dependent effects beyond the Born-Oppenheimer approximation. This simulation tool applies well-known thermodynamic equations to derive the Debye temperature (θ_D) and the out-of-equilibrium Gibbs function G*(V, P, T).

The Debye model [29] provides an essential framework for estimating phonon behavior in solids by modeling the material as a homogeneous, isotropic elastic medium. It assumes that sound waves travel without dispersion, leading to a linear relationship between frequency and wave vector (k). Within this model, the ($3p$) phonon branches where (p) denotes the number of atoms per unit cell are approximated as three acoustic modes, described by ($\omega = C_D\ k$), where (C_D) represents the velocity of sound. Given that a crystal consists of ($3pN$) total vibrational modes, where (N) is the number of primitive unit cells, the phonon density of states follows accordingly.

$$g_{Debye}(\omega) = \begin{cases} {}^{9n\omega^2}/_{\omega_D^3} & si\ \omega < \omega_D \\ 0 & si\ \omega \geq \omega_D \end{cases} \quad (1)$$

Here, n represents the unit cell density, while ω_D is the Debye frequency associated with the Debye.

$$\theta_D = \frac{\omega_D}{K_B} = \frac{1}{K_B}\left(\frac{6\pi^2 n}{V}\right)^{\frac{1}{3}} \upsilon_0 \quad (2)$$

where υ_0 is the mean velocity of the three acoustic phonon branches. In this model, the Grüneisen parameter γ is given by:

$$\gamma = -\frac{\partial \ln \theta_D}{\partial \ln V} \quad (3)$$

Thermodynamic parameters extracted from $g_{Debye}(\omega)$ comprise Helmholtz free energy (F), entropy (S), heat capacities (C_V and C_P), and the thermal expansion coefficient (α), offering valuable insights into the material's thermal characteristics.

$$F = E_{sta}(x, V) + \frac{9}{8} nK_B\theta_D + 3nK_B T \ln\left(1 - e^{-\theta_D/T}\right) - nK_B T D\left(\frac{\theta_D}{T}\right) \quad (4)$$

$$S = -3nK_B \ln\left(1 - e^{-\theta_D/T}\right) + 4nK_B D\left(\frac{\theta_D}{T}\right) \quad (5)$$

$$C_V = 12nK_B D(\theta_D/T) - \frac{9nK_B\theta_D/T}{e^{\theta_D/T} - 1} \quad (6)$$

$$C_p = C_v(1 + \alpha\gamma T) \quad (7)$$

$$\alpha = -\frac{1}{V}\left(\frac{\partial V}{\partial T}\right)_P = \frac{\gamma\, C_V}{B_T V} \quad (8)$$

Here, (B_T) represents the isothermal bulk modulus, (n) corresponds to the number of atoms per unit cell, and ($D(x)$) signifies the Debye integral.

$$D(x) = \frac{3}{x^3}\int_0^x \frac{y^3 e^y}{1 - e^y}\, \partial y \quad (9)$$

The elastic constants, which are important in the evaluation of the stability and mechanical behavior of materials, were calculated using the Iterative Relaxation of Atomic Structure (IRELAST) method [30] within WIEN2k code. Through the application of small strains on the crystal lattice and the analysis of stress tensors, the elastic constants were calculated which include (bulk modulus, shear modulus, Young's modulus) and were obtained through the application of the IRELAX method on the atoms, under the WIEN2k framework. Through these accurate calculations, the mechanical properties of SnMSiH (M = Al, Ga) hydrides are characterized for technological applications.

3 | Results and Discussion

3.1 | Structural Properties

This study presents a pioneering investigation into the structural properties of SnMSiH compounds (where M = Al or Ga), marking the first exploration of these materials. By extending prior research on complex hydrides, we analyze the crystallization tendencies of these compounds, which are expected to adopt a hexagonal lattice. Computational modeling suggests that this structural arrangement could facilitate unique electronic interactions, potentially enhancing hydrogen storage via unconventional atomic bonding mechanisms.

Prior research on AB_2H_2-type compounds has confirmed their stability in the hexagonal P3m1 structure, characterized by B atoms arranged in graphitic-like layers coordinated by three adjacent *A* atoms, with hydrogen occupying specific interstitial sites [18, 19]. Based on these established structural precedents, we hypothesize that the SnMSiH (M = Al, Ga) compounds investigated in this work will adopt an analogous configuration. Confirming this structural resemblance is critical, as it would provide a foundational framework for understanding the hydrogen storage mechanisms in these materials. Specifically, it would enable a direct analysis of how the local atomic environment—dictated by the nature of the M atom and the Sn-H interactions within this prototype structure—governs key properties such as hydrogen binding energies and diffusion pathways, thereby offering valuable insights for material design.

This study specifically examines the spatial distribution of Sn, M (Al, Ga), and H atoms within the crystalline unit, the influence of metal cations (Al^{3+} vs. Ga^{3+}) on structural stability, and the correlation between electronic configurations and hydrogen storage potential. These factors are essential in determining the thermodynamic stability of the hexagonal lattice. Crystallographic analysis, as depicted in Figure 1, and presented in Table 1 confirm the P3m1 space group (No. 156) for SnMSiH compounds, validating their structural feasibility. These findings contribute to the development of novel hydrogen storage materials aligned with clean energy technologies.

To evaluate the stability and structural properties of SnAlSiH and SnGaSiH, total energy calculations were performed using the Murnaghan equation of state [31]. The energy volume dependence was determined using both generalized gradient approximation (GGA) and local density approximation (LDA). The computed lattice parameters (a, c), c/a ratios, bulk moduli (B), pressure derivatives (B′), and unit cell volumes (V) are presented in Table 2.

For SnAlSiH, LDA calculations yielded lattice parameters a = 4.14673 Å and c = 5.88394 Å, with a c/a ratio of 1.4189, whereas GGA predicted a = 4.15533 Å and c = 5.84491 Å (c/a = 1.4066). Both methods produced a unit cell volume of approximately 87.4 $Å^3$, with bulk modulus values of 52.53 GPa (GGA) and 52.77 GPa (LDA). Conversely, SnGaSiH exhibited a pronounced lattice expansion due to Ga's larger atomic radius. LDA calculations yielded a = 4.19022 Å and c = 5.98367 Å (c/a = 1.4280), while GGA estimated a = 4.24699 Å and c = 5.87988 Å (c/a = 1.3845). The unit cell volume increased to ~91.85 $Å^3$ (GGA) and 90.99 $Å^3$ (LDA), while the bulk modulus decreased to 46.20 GPa (GGA) and 47.68 GPa (LDA).

This variation underscores the impact of substituting Al with Ga: Ga's larger atomic radius induces lattice expansion, thereby reducing mechanical stiffness (lower B) while maintaining structural stability. Differences in c/a ratios between LDA and GGA highlight the role of exchange-correlation interactions in crystallographic predictions. The lower bulk modulus of SnGaSiH suggests a softer lattice, which may enhance hydrogen diffusion kinetics an essential attribute for hydrogen storage applications. Lattice expansion in Ga-substituted compounds further illustrates the relationship between atomic size, electronic interactions, and structural flexibility, critical for optimizing hydrogen absorption and desorption properties.

Table 3 provides insight into the atomic bonding characteristics of SnAlSiH and SnGaSiH. The Al–H bond lengths in SnAlSiH were found to be 1.78 Å (GGA) and 2.42 Å (LDA), indicating notable variations due to different exchange-correlation treatments. In contrast, SnGaSiH exhibited relatively stable Ga–H bonds (~1.72 Å), which may contribute to enhanced material stability. The core atoms (Al/Ga) significantly influence interatomic distances, as reflected in the Ga–Si bond range (2.40–2.46 Å) and the X–Si bond range (3.33–3.55 Å for SnAlSiH and 3.12–3.53 Å for SnGaSiH).

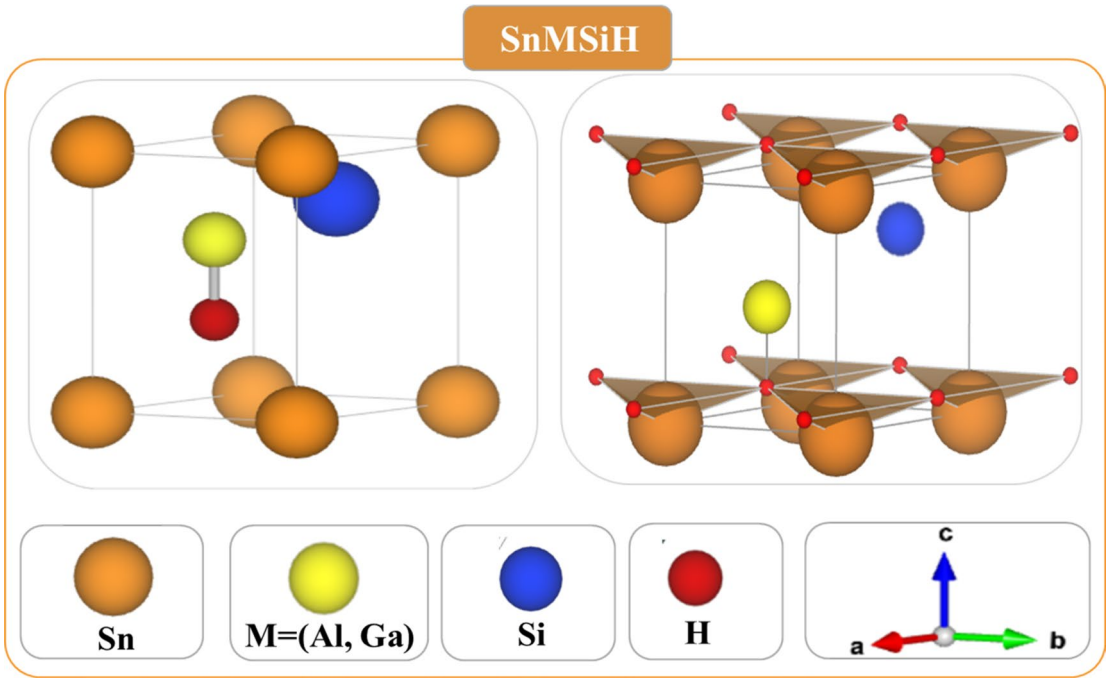

FIGURE 1 | Crystal structures of Hexagonal SnMSiH, with M encompassing Aluminum (Al) and Gallium (Ga).

TABLE 1 | Atomic positions of SnAlSiH and SnGaSiH compounds.

Hydrids	Atomic positions (*z*)		
	(*x y z*)	GGA	LDA
SnAlSiH P3m1	Sn (0 0 0 z)	0.8392	0.8274
	Al (2/3 1/3 z)	0.4869	0.4879
	Si (1/3 2/3 z)	0.6303	0.6407
	H (2/3 1/3 z)	0.1816	0.1845
SnGaSiH P3m1	Sn (0 0 0 0)	0.1935	0.1970
	Ga (2/3 1/3 z)	0.5121	0.5163
	Si (1/3 2/3 z)	0.3549	0.3482
	H (2/3 1/3 z)	0.8121	0.8132

TABLE 2 | Lattice constants (in Å), bulk modulus (in GPa), and pressure derivative (B′) at equilibrium volume, determined using GGA and LDA for SnAlSiH and SnGaSiH compounds.

Compounds (structure type; space group)	Lattice parameters		
		GGA	LDA
SnAlSiH P3m1	a	4.1553	4.1467
	c	5.8449	5.8839
	c/a	1.4066	1.4189
	B(Gpa)	52.5273	52.7700
	B′	4.3524	4.3888
	V(Å^3)	87.402	87.621
SnGaSiH P3m1	a	4.2469	4.1902
	c	5.8798	5.9836
	c/a	1.3844	1.4280
	B(Gpa)	46.2039	47.6809
	B′	4.5637	4.5994
	V(Å^3)	91.8464	90.9855

Furthermore, structural angles such as Ga–Si–Ga and Si–Ga–Si in SnGaSiH ranged from 114.5° to 115.8°, indicating minor distortions in the hexagonal P3m1 lattice. The Si–Ga–H angle (103.8° in SnGaSiH vs. 102° in SnAlSiH) suggests that Ga's larger atomic radius influences local charge distributions. These subtle geometric modifications contribute to the increased compressibility of SnGaSiH, further reducing its bulk modulus.

The composition-dependent variations in atomic bonding and lattice geometry emphasize the role of constituent elements in optimizing material properties for hydrogen storage. The stability of Ga–H bonds across different approximations, along with the observed structural flexibility, highlights the potential of SnMSiH compounds for next-generation hydrogen storage applications.

3.2 | Electronic Properties and Density Charge

The electronic structure of SnMSiH (M = Al, Ga) compounds in the primitive hexagonal crystal structure (P3m1) was determined using GGA, functionals. The electronic band structure, shown in Figure 2, reveals that both compounds exhibit semimetallic behavior, as evidenced by the absence of an energy gap at the Fermi level (E_F) and the direct overlap of valence and conduction bands. Notably, portions of the valence band extend above the Fermi level along high-symmetry directions in the Brillouin zone, while the conduction band intersects E_F, facilitating charge carrier transport with minimal activation energy.

The semi-metallic character of these SnMSiH compounds originates from direct band crossings along specific high-symmetry directions in the Brillouin zone, a phenomenon observed in prototypical semi-metals such as graphene and bismuth. This electronic structure results in a negligible band gap and a continuous density of states at the Fermi level, facilitating a seamless flow of charge carriers. We posit that this enhanced electronic conductivity strengthens the interaction between the host lattice and hydrogen atoms, potentially improving charge transfer during the sorption process. This mechanism is anticipated to be highly advantageous for hydrogen storage, as it could lower the kinetic energy barriers for both hydrogen absorption and desorption, irrespective of whether the primary interactions are

TABLE 3 | Atomic bond lengths (Å) and bond angles (°) in SnMSiH (X = Al, Ga) compounds.

SnAlSiH	GGA	LDA	SnGaSiH	GGA	LDA
Al-H (×3)	1.7847	1.7848	**Ga-Si (×3)**	1.7640	1.7766
Sn1-Sn1 (×3)	4.1553	4.1467	**X-H (×3)**	4.2469	4.1902
Sn1-Si1 (×3)	2.6919	2.6340	**X-Si (×3)**	2.6291	2.5828
Si1-Al1 (×3)	2.5411	2.5575	**X-Ga (×3)**	2.6205	2.6200
H1-Sn1 (×1)	3.1242	3.1854	**Ga-H (×1)**	3.3227	3.3356
Ga-Si-Ga (×3)	109.6913	108.3283	**Ga-Si-Ga (×3)**	108.2569	106.1951
Si-Ga-Si (×3)	109.6913	108.3283	**Si-Ga-Si (×3)**	108.2569	106.1951
Si-Ga-H (×3)	109.2501	110.5912	**Si-Ga-H (×3)**	110.6597	112.5766

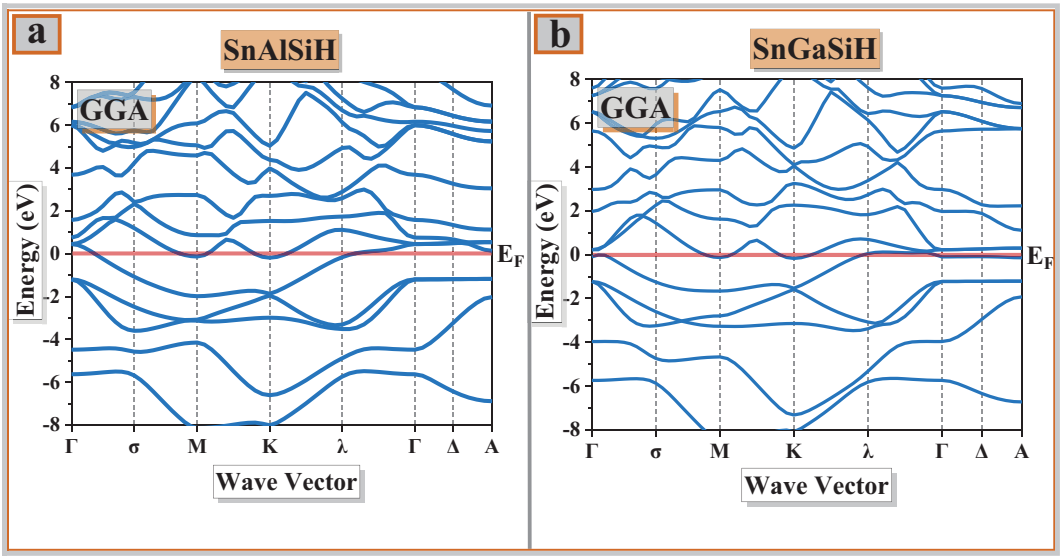

FIGURE 2 | Band structure for (a) SnAlSiH and (b) SnGaSiH compounds, computed using GGA.

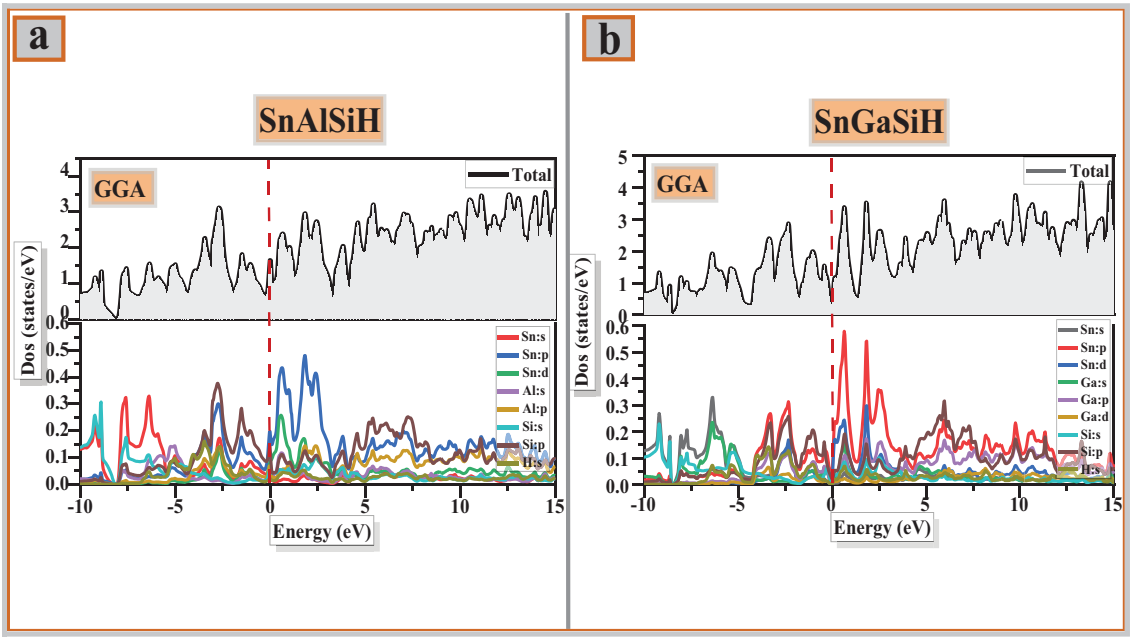

FIGURE 3 | The density of states (DOS) for: (a) SnAlSiH and (b) SnGaSiH compounds, calculated using GGA.

chemical (Kubas-type) or physical in nature. Consequently, the inherent semi-metallicity of SnMSiH Zintl phases establishes them as a promising material platform for achieving both high hydrogen capacity and favorable sorption kinetics, which are critical for the development of advanced solid-state hydrogen storage systems.

The electronic density of states (DOS), illustrated in Figure 3, highlights differences between SnAlSiH and SnGaSiH due to variations in orbital interactions. In SnAlSiH, the deep energy region (−10 eV to −5 eV) is primarily composed of contributions from the Al-s and Si-s orbitals, while the region near the Fermi level (−5 eV to 0 eV) is dominated by Si-p and Sn-d states, with weak Al-p contributions. This results in a zero-energy gap, confirming the semi-metallic nature of SnAlSiH. Conversely, SnGaSiH exhibits stronger Ga-p and Si-p interactions, leading to the emergence of a small energy gap (0.2–0.3 eV). The presence of Ga enhances electron dispersion near the Fermi level, making the material more ductile, as indicated by the lower bulk modulus ($B \approx 46$ GPa for SnGaSiH compared with 52 GPa for SnAlSiH).

Additionally, the larger atomic radius of Ga increases the unit cell volume (91.8 Å^3 for SnGaSiH vs. 87.4 Å^3 for SnAlSiH). The bonding interactions between Ga, Si, and the hydrogen s-orbital contribute to the structural stability of SnGaSiH, making it a viable candidate for hydrogen storage applications. Meanwhile, the medium-range electronic conductivity of SnAlSiH suggests its suitability for sensor applications. On the other hand, the small energy gap and strong structural stability of SnGaSiH make it a promising candidate for optoelectronic applications such as

solar cells and photodetectors. These findings underscore the importance of compositional tuning to develop functional materials for energy applications.

Figure 4 presents the electronic charge density distribution in the (110) crystallographic plane for SnAlSiH and SnGaSiH. This plane is particularly significant in hexagonal structures as it includes key atomic bonding interactions, allowing for a detailed analysis of charge distribution variations due to Al/Ga substitution. In SnAlSiH, the charge concentration around Al is lower than around Ga in SnGaSiH, indicating a more ionic bonding character. While the charge distribution around Si remains relatively constant, the reduced charge density near Al suggests weaker orbital overlap with neighboring atoms. In contrast, SnGaSiH exhibits a notable increase in charge concentration around Ga, indicative of a stronger covalent bonding character. The higher charge localization around Ga is consistent with its greater electronegativity compared with Al, leading to enhanced covalent interactions and increased polarization of the electronic cloud. Since the (110) plane encompasses all chemically active atoms in the hexagonal lattice, it serves as an ideal reference for analyzing these bonding changes. The stronger ionic nature of SnAlSiH may facilitate hydrogen adsorption and desorption, whereas the enhanced covalent bonding in SnGaSiH could lead to stronger hydrogen retention within the lattice, potentially hindering its release. These findings offer essential guidance for enhancing SnMSiH compounds in hydrogen storage and other energy-related applications.

3.3 | Thermodynamic Properties

Figures 5–10 illustrate the thermal properties of SnAlSiH and SnGaSiH compounds, highlighting the effects of substituting aluminum with gallium on their structural and thermodynamic behavior. Figure 5 illustrates that the equilibrium volume of both compounds rises with increasing temperature, especially at low pressure (0 GPa), where SnGaSiH exhibits ~5% more expansion than SnAlSiH. This expansion is attributed to the larger atomic radius of gallium, which enhances the crystalline flexibility of the compound. At higher pressures (40 GPa), thermal expansion diminishes due to atomic compression. However, SnGaSiH retains a greater capacity to accommodate thermal stresses, making it more suitable for dynamic applications.

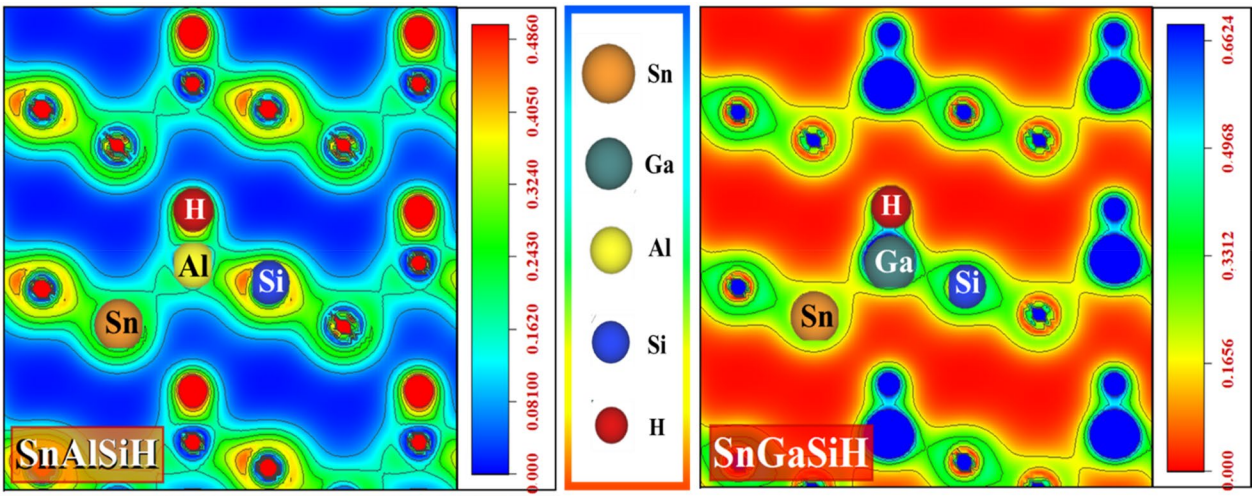

FIGURE 4 | Contour plot of total valence charge density distributions in the (110) plane using the GGA approximation for SnAlSiH and SnGaSiH compounds.

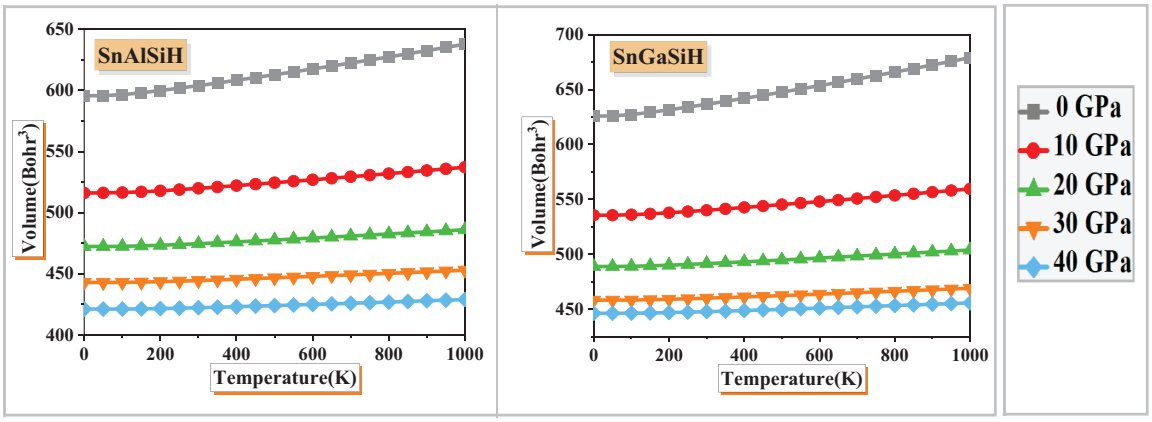

FIGURE 5 | Variation of the volume cell as a function of the temperature for SnAlSiH and SnGaSiH at different pressures, using GGA.

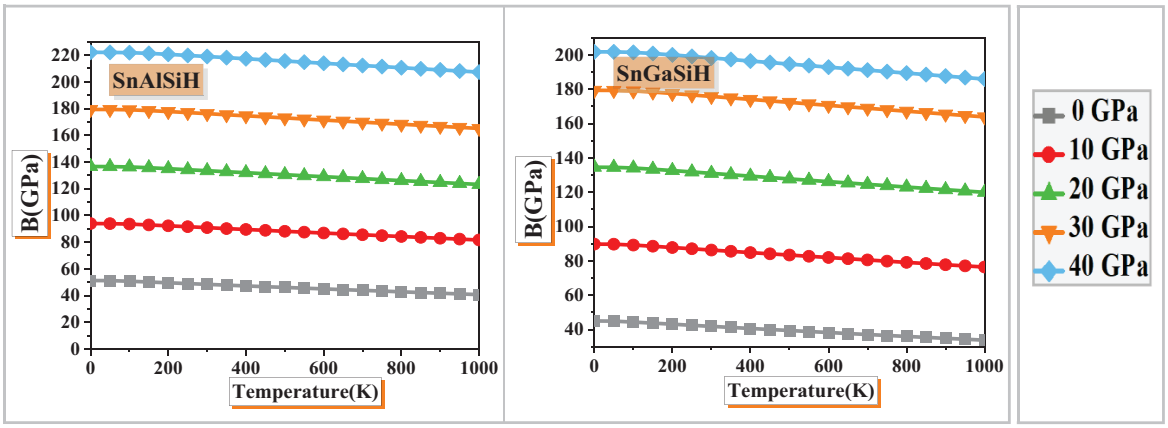

FIGURE 6 | Variation of the bulk modulus as a function of the temperature for SnAlSiH and SnGaSiH at different pressures, using GGA.

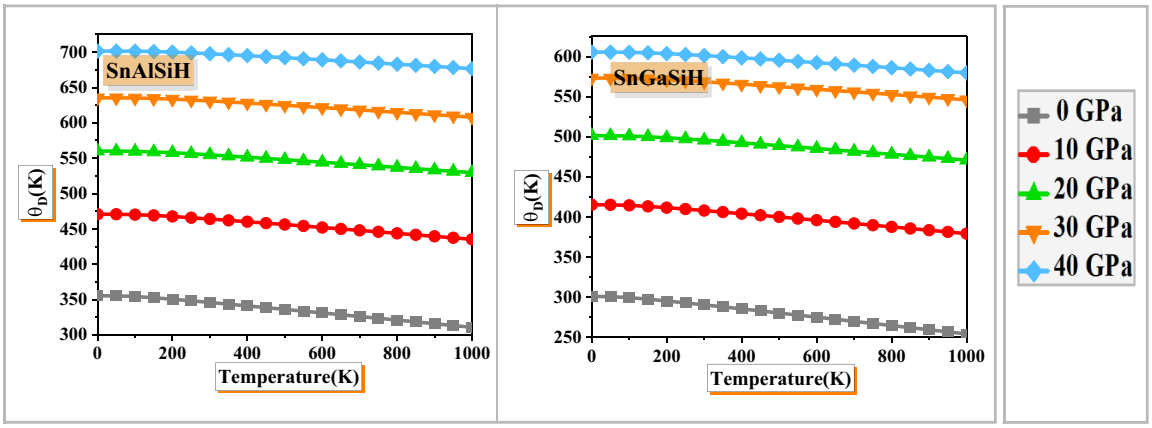

FIGURE 7 | Variation of the Debye temperature θ_D as a function of the temperature for SnAlSiH and SnGaSiH at different pressures, using GGA.

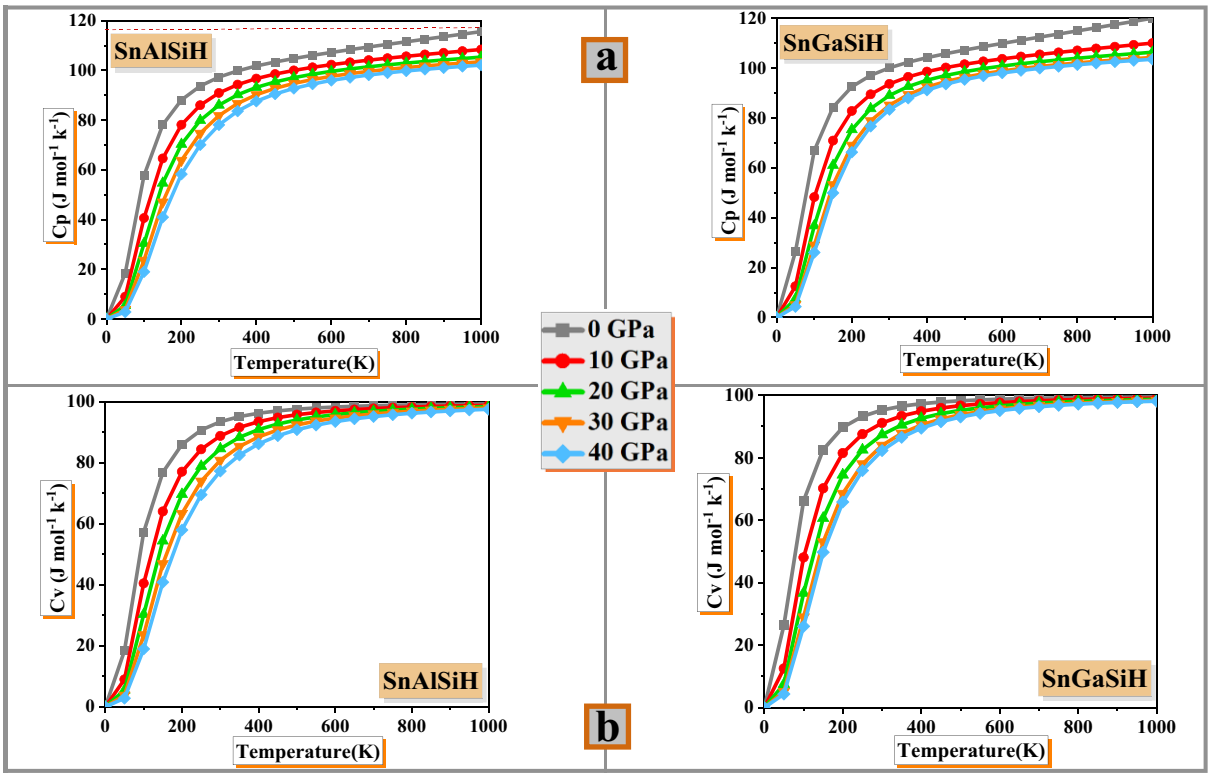

FIGURE 8 | Variation of (a): The heat capacity Cp and (b): The heat capacity C_v as a function of temperature for SnAlSiH and SnGaSiH at different pressures, using GGA.

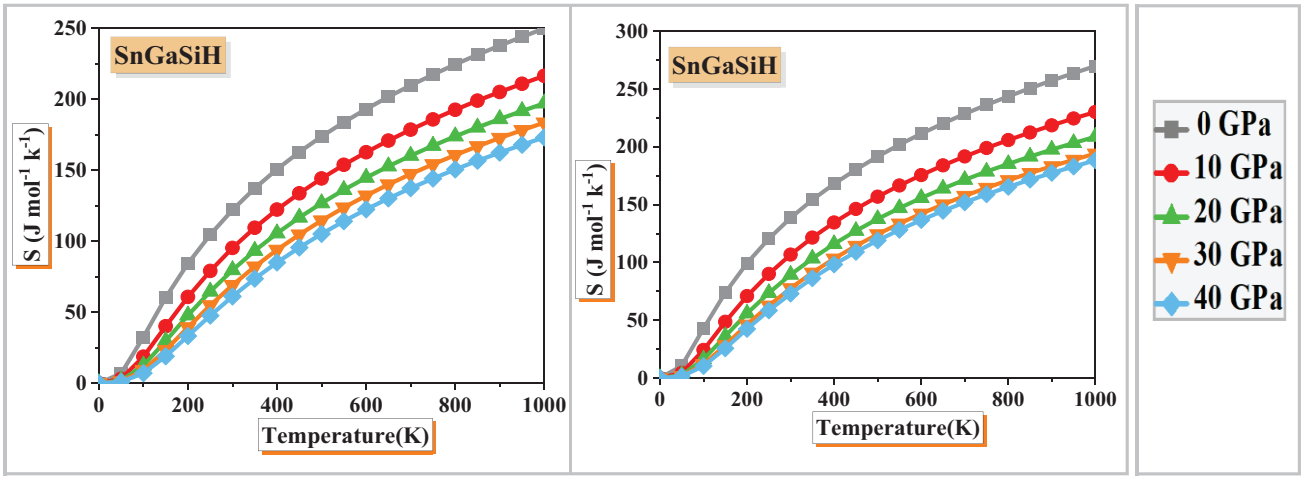

FIGURE 9 | Variation of the entropy S as a function of the temperature for SnAlSiH and SnGaSiH at different pressures, using GGA.

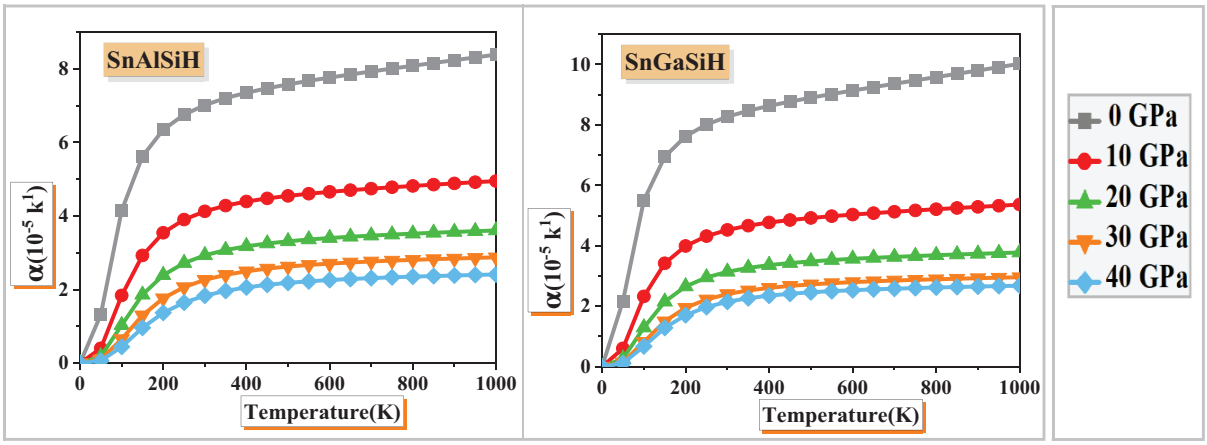

FIGURE 10 | Variation of thermal expansion α as a function for SnAlSiH and SnGaSiH at different pressures, using GGA.

At 0 K, the bulk modulus of SnGaSiH is 46 GPa, compared with 52 GPa for SnAlSiH, indicating that SnGaSiH exhibits higher compressibility and reduced rigidity. As illustrated in Figure 6, the bulk modulus decreases linearly with increasing temperature, reflecting the softening of the material under thermal influence. At 40 GPa, the rigidity of SnGaSiH increases to 85 GPa, while SnAlSiH reaches 92 GPa, confirming that the latter maintains greater structural stability under high-pressure conditions.

The Debye temperature (θ_D), a key indicator of lattice vibrations and bonding strength, is presented in Figure 7. At 0 K, θ_D for SnGaSiH is 335 K, while SnAlSiH exhibits a higher θ_D of 375 K, signifying stronger interatomic bonding in the latter. However, at 40 GPa, θ_D for SnGaSiH rises to 400 K, indicating improved thermal stability under high-pressure conditions.

The heat capacity at constant pressure (Cp), depicted in Figure 8a, reaches 105 J mol^{-1} K^{-1} at 300 K for SnGaSiH, compared with 98 J mol^{-1} K^{-1} for SnAlSiH. This suggests that SnGaSiH has a greater ability to absorb and release heat, which is advantageous for hydrogen storage applications where thermal regulation is critical. At higher temperatures, Cp values align with Dulong Petit's law, which states that heat capacity approaches a constant value as all vibrational degrees of freedom become fully activated.

Figure 8b presents the heat capacity at constant volume (C_v), demonstrating that at low temperatures (< 200 K), C_v follows a T^3 dependence due to dominant acoustic phonon contributions. At higher temperatures, deviations arise due to optical phonon interactions. The structural flexibility of SnGaSiH allows for a more rapid increase in C_v, enhancing its thermal response characteristics.

As temperature increases, the entropy (S) of both compounds also rises, as illustrated in Figure 9. At 1000 K, S reaches 180 J mol^{-1} K^{-1} for SnGaSiH, compared with 165 J mol^{-1} K^{-1} for SnAlSiH. This higher entropy in SnGaSiH suggests greater atomic mobility and structural disorder, which could facilitate hydrogen diffusion within the lattice. Unlike SnAlSiH, which exhibits metallic-like behavior, SnGaSiH has a higher density of electronic states near the Fermi level, characteristic of its semiconducting nature and weaker atomic interactions.

Figure 10 shows the thermal expansion coefficient (α), which is 9.8×10^{-5} K^{-1} for SnGaSiH at 0 GPa and 300 K, compared with

$8.2\times10^{-5}\,K^{-1}$ for SnAlSiH. The higher α value for SnGaSiH is attributed to enhanced anharmonic vibrations, which promote the formation of interstitial spaces crucial for hydrogen storage. At 40 GPa, α decreases for both compounds due to restricted atomic mobility under high-pressure conditions.

The thermodynamic properties of these compounds reveal their suitability for different energy-related applications. SnGaSiH's lower bulk modulus facilitates easier hydrogen absorption and release, while its strong thermal expansion at low pressures enhances hydrogen uptake. Additionally, its higher C_p enables efficient thermal management, reducing the risk of heat accumulation during hydrogen interaction processes. The increased entropy in SnGaSiH further supports hydrogen mobility, making it a promising candidate for hydrogen storage.

Conversely, SnAlSiH demonstrates superior thermal stability, as evidenced by its higher Debye temperature (θ_D), and enhanced mechanical rigidity, indicated by its larger bulk modulus. These properties suggest a stronger bonding network and greater resistance to structural deformation under stress, rendering it more suitable for applications where structural robustness and long-term mechanical durability are paramount.

These comparative findings highlight that gallium substitution serves as an effective strategy for tuning the functional properties of Zintl-phase hydrides. The distinct performance profiles of these compounds enable targeted application: SnGaSiH is optimal for systems requiring rapid hydrogen cycling and efficient thermal management, whereas SnAlSiH is better suited for high-pressure or mechanically demanding environments. This structure–property relationship provides a valuable design principle for engineering next-generation hydrogen storage materials with customized performance characteristics.

3.4 | Hydrogen Storage Properties

Gravimetric hydrogen storage capacity (Cw%) is a crucial parameter for determining a material's viability in hydrogen storage applications, including fuel cells and hydrogen-powered vehicles. Expressed in weight percent (wt%), it quantifies the amount of hydrogen stored relative to the material's total mass. Recent studies on hydride-based materials like SnMSiH (M = Al, Ga) have utilized Equation (10) from Ref. [32] to calculate hydrogen storage capacities based on experimental data.

$$\mathrm{CW}\,\% = \left(\frac{\left(\frac{H}{M}\right) M_H}{M_{\mathrm{Host}} + \left(\frac{H}{M}\right) M_H} \times 100 \right) \% \tag{10}$$

where M_H stands for hydrogen mass and M_{Host} for the molar mass of the host material. Using this formula, the study found that the gravimetric capacities of SnAlSiH and SnGaSiH were 0.58 wt% and 0.47 wt%, respectively, indicating the percentage of each compound's total weight that was contributed by hydrogen. These figures highlight how well the materials store hydrogen and provide crucial information for maximizing their incorporation into workable storage solutions [32, 33]. The process emphasizes how accurate gravimetric analysis advances materials for use in sustainable energy applications.

A material's ability to host hydrogen is indicated by its hydrogen to material atomic ratio (H/M), which measures the percentage of hydrogen atoms in relation to the material's overall atomic composition. The mass of absorbed hydrogen is denoted by H in hydrogen storage devices, and the mass of the host material and stored hydrogen is denoted by M. In this case, M_H (the molar mass of hydrogen) makes it easier to convert between the mass and atomic count of hydrogen, while M_{Hhost} denotes the molar mass of the host material minus hydrogen.

A crucial criterion for assessing storage efficiency in systems like fuel cells, the hydrogen content per unit mass can be precisely determined thanks to these characteristics [32, 33]. The desorption temperature (T_D), the point at which heating causes hydrogen to be released, is equally important because it has a direct bearing on the security and effectiveness of storage systems. Equation (11) in Ref. [34] is the Gibbs-Helmholtz equation, from which the following is derived:

$$\Delta S = \frac{\Delta H - \Delta G}{T} \tag{11}$$

where enthalpy change, entropy change, and Gibbs free energy change are shown by the symbols ΔG, ΔH, and ΔS, respectively. The formula for T_D at equilibrium ($\Delta G = 0$) is [35]:

$$T_D = \frac{\Delta \mathrm{H}}{\Delta S} \tag{12}$$

The thermodynamic properties of hydrogen desorption play a vital role in evaluating a material's potential for hydrogen storage applications. Unlike the negative enthalpy of formation associated with material synthesis, the enthalpy change (ΔH) for dehydrogenation is typically positive, reflecting its endothermic nature. This distinction underscores the need for precise thermodynamic analysis to optimize material performance. By integrating gravimetric capacity measurements with desorption behavior, researchers can comprehensively evaluate materials like SnAlSiH and SnGaSiH for sustainable energy applications [32–35].

The Gibbs-Helmholtz equation establishes a fundamental link between enthalpy (ΔH), entropy (ΔS), and desorption temperature (T_D), offering valuable insights into the conditions required for hydrogen release. Given that dehydrogenation generally requires heat input, a higher ΔH correlates with increased thermal energy demands. The associated entropy change (ΔS) quantifies the degree of disorder introduced during hydrogen release, influencing the reaction's thermodynamic favorability.

Using this framework, the desorption temperatures and entropy changes were determined as $T_D = 310.69$ K, $\Delta S = 249.90$ J/mol·K for SnAlSiH and $T_D = 254.15$ K, $\Delta S = 269.86$ J/mol·K for SnGaSiH. The lower desorption temperature of SnGaSiH

suggests that hydrogen can be released under milder conditions, potentially enhancing storage system efficiency. Additionally, its higher entropy change implies greater atomic rearrangement upon hydrogen release, which may improve dehydrogenation kinetics. In contrast, SnAlSiH, with a higher T_D, requires more heat for hydrogen desorption, which could impact its applicability in specific storage configurations.

While the calculated gravimetric hydrogen storage capacities of SnAlSiH (0.58 wt%) and SnGaSiH (0.47 wt%) are significantly below the U.S. DOE 2025 system-level target of 5.5 wt% [Citation DOE], they should not be viewed in isolation. The primary value of this study lies in establishing the fundamental viability of this Zintl phase hydride platform. The computed properties—including their inherent thermodynamic stability, semi-metallic character, and tunable mechanical properties (e.g., enhanced ductility with Ga substitution)—are critical prerequisites for any practical material. These traits suggest a system capable of reversible hydrogenation and good cycle life. The challenge, therefore, is not one of fundamental suitability but of capacity engineering. The relatively low capacity is primarily a function of the high atomic mass of the constituent Sn and Ga/Al atoms; thus, the pathway to improvement lies in strategic compositional light-weighting while preserving the advantageous Zintl structure and electronic properties.

The analysis herein utilizes bulk thermodynamic approximations to provide an initial estimate of hydrogen storage potential. It is imperative to state that these values, particularly the desorption temperatures, are inherently speculative in the absence of mechanistic calculations at the atomistic level. A reliable assessment mandates future investigation into the following properties for these systems: the definitive identification of hydrogen incorporation sites, the calculation of absolute hydrogen binding energies (E_b), the determination of diffusion energy barriers (E_a) via the Nudged Elastic Band (NEB) method, and a rigorous evaluation of the thermodynamic stability of the ternary hydride against decomposition into binary phases (e.g., SnH_4, AlH_3, SiH_4). The principal contribution of this work is to demonstrate that the SnAlSiH and SnGaSiH Zintl phases possess the fundamental host properties—structural, electronic, and mechanical—that constitute a necessary and justified prerequisite for such a computationally intensive study. The preliminary metrics presented here serve to identify these compounds as promising candidates for that subsequent essential research.

3.5 | Elastic Properties

Elastic constants play a key role in analyzing the mechanical and dynamic properties of solid materials. They offer valuable information about a material's inherent rigidity, structural stability, and the internal interactions shaping its crystalline framework. These parameters are essential for predicting material stability, deformation resistance, and the ability to recover its original shape after stress is removed.

The accurate determination of elastic constants requires robust mathematical models of atomic interactions, typically employing first- and second-order potential functions to describe the response of the crystal lattice to strain. These models are implemented within ab initio computational frameworks, which derive elastic properties directly from quantum mechanical principles, free of empirical parameters. For instance, the WIEN2k code utilizes force-based algorithms to achieve high-precision structural optimization and subsequent calculation of the elastic tensor. Despite the predictive power of these theoretical methods, the experimental validation of single-crystal elastic constants remains a significant challenge, often constrained by measurement limitations and the demand for extreme accuracy in sample preparation and data collection [36].

The mechanical behavior of hexagonal systems, including SnMSiH compounds, is characterized by six independent elastic constants: C_{11}, C_{12}, C_{13}, C_{33}, C_{44}, and C_{66}. Specifically, C_{11} and C_{33} describe compressibility along principal crystallographic directions, C_{12} and C_{13} govern the coupling between deformations along different axes, while C_{44} and C_{66} reflect the material's shear resistance. These constants must be found by examining energy changes under applied pressures, which calls for a significant amount of computing power and in-depth analyses of the crystal's reaction.

By monitoring strain responses to controlled stresses, the stress–strain approach helps further in the derivation of elastic constants. This method uses metrics like C_{ij}. The creation of hexagonally structured materials for uses ranging from energy storage to aeronautical engineering is advanced by tools like WIEN2K, which improve such assessments by permitting accurate lattice modeling.

According to equation (13) [37], the compounds SnAlSiH and SnGaSiH display positive elastic constants (C_{11}, C_{33}, C_{44}, and C_{66}), demonstrating their mechanical stability. These results are shown in Table 4 for the hexagonal crystal structure (space group P3m1).

$$\begin{cases} C_{44} > 0, C_{66} > 0, C_{11} > |C_{12}| \\ C_{11}C_{33} > C_{13}^2 \\ (C_{11} + C_{12})C_{33} - 2C_{13}^2 > 0 \end{cases} \tag{13}$$

Because SnAlSiH records higher values for the majority of the elastic constants than SnGaSiH (e.g., $C_{11} = 91.689$ GPa vs.

TABLE 4 | Elastic constants of SnMSiH (X = Al, Ga) computed using the GGA approach.

Compounds	SnAlSiH P3m1	SnGaSiH P3m1
C_{11}	91.6891	81.0785
C_{33}	50.1584	43.4523
C_{44}	29.7230	22.2215
C_{66}	15.6989	10.5842
C_{12}	60.2913	59.9101
C_{13}	37.4376	29.231
T_m	1044.1186 ± 300	978.0235 ± 300
A_1	1.7752	1.35492
A_2	1	1

81.078 GPa), the arrangement of the elastic constants shows the superior hardness of SnAlSiH and indicates greater resistance to bulk and shear deformation. Deformation along the c-axis is easier than along the a-axis because of the lower atomic density in the vertical direction, as evidenced by the fact that the vertical compression constant (C_{33}) is lower than the horizontal one (C_{11}) in both compounds (e.g., $C_{33} = 50.158$ GPa for SnAlSiH vs. $C_{11} = 91.689$ GPa). SnAlSiH has higher values for C_{44} (29.723 GPa) than SnGaSiH (22.221 GPa) in terms of shear resistance, indicating greater resistance to deformation in the (001) plane.

Conversely, in both compounds, C_{66} exhibits lower values (15.698 GPa and 10.584 GPa, respectively), suggesting that shear deformation in the (100) plane is simpler. While the {001} plane shows isotropy ($A_2 = 1$), the anisotropy factors ($A_1 = 1.775$ for SnAlSiH and 1.354 for SnGaSiH) confirm directional variation in shear resistance, especially in the {100} plane [37]. Regarding thermal characteristics, the formula $T_m = 607 + 9.3 \times B$ [38] links the melting temperature (T_m) to the bulk modulus (B). The larger B values deduced from the elastic constants are consistent with the higher melting temperature of SnAlSiH (1044.12 ± 300 K) compared with SnGaSiH (978.02 ± 300 K). This discrepancy illustrates how SnAlSiH has stronger atomic bonds, which make it more stable in extremely hot environments [39].

For the compounds under study, the bulk modulus ordering is as follows: SnAlSiH ($B = 55.985$ GPa) > SnGaSiH ($B = 49.254$ GPa). SnGaSiH is anticipated to degrade at a lower temperature than SnAlSiH due to the observed correlation between bulk modulus and melting point. The Hill model [40, 41], which is an average of the findings from the Voigt model [42] and the Reuss model [43], was used to calculate the shear modulus (G) and bulk modulus (B). In particular, the following values were found for hexagonal systems: Hill shear modulus (G_H), Hill bulk modulus (B_H), Reuss shear modulus (G_R), Reuss bulk modulus (B_R), and Voigt shear modulus (G_V) and (B_V).

$$B_V = \frac{2C_{11} + 2C_{12} + 4C_{13} + C_{33}}{9} \tag{14}$$

$$B_R = \frac{(C_{11} + C_{12})C_{33} - 2C_{13}^2}{C_{11} + C_{12} - 4C_{13} + 2C_{33}} \tag{15}$$

$$G_V = \frac{4C_{11} + 2C_{33} - 4C_{13} - 2C_{12} + 12C_{44} + 6C_{66}}{30} \tag{16}$$

$$G_R = 15\left(\frac{4C_{11} + 4C_{12} + 8C_{13} + 2C_{33}}{(C_{11} + C_{12})C_{33} - 2C_{13}^2} + \frac{6}{C_{11} - C_{12}} + \frac{6}{C_{44}} + \frac{3}{C_{66}}\right)^{-1} \tag{17}$$

$$B_H = \frac{1}{2}(B_V + B_R) \tag{18}$$

$$G_H = \frac{1}{2}(G_V + G_R) \tag{19}$$

The elastic properties of composite materials are evaluated using the Voigt and Reuss models; the former assumes uniformity of structure and gives the upper limit of stiffness, while the latter assumes multiphase and gives the lower limit. Actual values often fall in between, so the average Hill is used to achieve a more accurate and realistic assessment.

The following formulas are used to determine Poisson's ratio (σ) and Young's modulus (E) [44]:

$$\begin{cases} E = \dfrac{9\,B\,G}{(G + 3B)} \\ \sigma = \dfrac{3B - 2G}{2(3B + G)} = \dfrac{1}{2}\left(1 - \dfrac{E}{3B}\right) \end{cases} \tag{20}$$

Research in Ref. [45] indicates that SnMSiH materials (M = Al, Ga) exhibit remarkably high compressibility, allowing significant deformation under applied stress. This characteristic is consistent with their low elastic moduli, which are significantly lower than those of conventional metals [46] and intermetallic compounds [47]. Despite their low resistance to deformation, SnMSiH compounds retain a unique mechanical adaptability, making them suitable for hydrogen storage applications where flexibility and compressive strength are crucial.

To evaluate ductility, the bulk-to-shear modulus ratio (B/G) is a key parameter, as per Pugh's criterion [48]. A material is considered ductile if $B/G > 1.75$, indicating its ability to deform without breaking. The SnMSiH compounds meet this criterion, with SnAlSiH showing stronger atomic bonding due to its higher bulk modulus ($B_V = 55.985$ GPa) compared with SnGaSiH ($B_V = 49.254$ GPa, Table 5).

Young's modulus (E) further characterizes a material's resistance to uniaxial deformation. A decrease in E_H from 53.707 GPa (SnAlSiH) to 41.944 GPa (SnGaSiH) reflects a significant reduction in hardness, making SnGaSiH more flexible under stress. This trend aligns with Poisson's ratio (σ), where SnAlSiH ($\sigma_H = 0.326$) and SnGaSiH ($\sigma_H = 0.343$) fall within the theoretical range for central bonds ($0.25 \leq \sigma \leq 0.5$) [49]. While both compounds exhibit volumetric stability during elastic deformation, SnGaSiH's slightly higher σ_H suggests greater lattice flexibility [50].

The bulk modulus (B_H) further confirms atomic bond strength, with SnAlSiH ($B_H = 51.493$ GPa) exceeding SnGaSiH ($B_H = 44.574$ GPa). These values align well with those derived from the equation of state (EOS) calculations using the GGA approximation, supporting the accuracy of the computed elastic constants (C_{ij}, Table 5).

With a volumetric anisotropy ratio (A_B%) of 10.50% and shear anisotropy (A_G%) of 7.53%, SnGaSiH has more directional variation in elastic anisotropy ($A^u = 1.048$) than SnAlSiH ($A^u = 0.898$), especially in the {100} and {001} planes. This is explained by variations in stress distribution brought forth by each compound's distinct crystal structure.

The mechanical properties of SnMSiH compounds suggest distinct application potentials. SnAlSiH, with higher hardness

TABLE 5 | Elastic moduli, sound velocities (longitudinal, transverse, and average), and Debye temperature of SnMSiH (M = Al, Ga) calculated using GGA.

	SnAlSiH	SnGaSiH		SnAlSiH	SnGaSiH
B_V (GPa)	55.985	49.254	B_H/G_H	2.5429	2.8546
B_R (GPa)	47.002	39.895	A_B %	8.7224	10.4971
B_H (GPa)	51.493	44.574	A_G %	6.6041	7.5283
G_V (GPa)	21.586	16.789	A^u	0.8982	1.0486
G_R(GPa)	18.912	14.439	$\nu_{t\ (m/s)}$	2469.34	1992.52
G_H (GPa)	20.249	15.614	$\nu_{l\ (m/s)}$	4861.74	4077.66
E_V (GPa)	57.382	45.228	$\nu_{m\ (m/s)}$	2767.53	2238.17
E_R (GPa)	50.026	38.653	θ_D(K)	294.725	234.443
E_H (GPa)	53.707	41.944			
σ_V	0.3291	0.3469			
σ_R	0.3226	0.3385			
σ_H	0.3261	0.3431			

($E_H = 53.707$ GPa) and greater resistance to deformation, is better suited for structural applications, whereas SnGaSiH, with higher flexibility ($\sigma_H = 0.343$), is more appropriate for dynamic applications requiring deformation absorption. The high B_H/G_H ratio (> 2.5) for both compounds confirms their flexibility, reducing the likelihood of fracture under cyclic loads [48].

Phase transitions in crystalline materials can be inferred from thermal conductivity tests [51], which relate to specific heat capacity through the Debye model. The Debye temperature (θ_D) plays a crucial role in understanding atomic bonding strength, as it correlates with elastic constants, heat capacity, and melting point [44]. At low temperatures, where acoustic vibrations dominate, θ_D can be estimated from elastic constants instead of direct heat capacity measurements. This involves computing the average sound velocity (v_m) using longitudinal (v_l) and transverse (v_t) wave velocities through established formulae [49–51].

$$\theta_D = \frac{h}{K_B}\left(\frac{3n}{4\pi}\left(\frac{N_a \rho}{M}\right)\right)^{\frac{1}{3}} \nu_m \tag{21}$$

where n is the number of atoms in the unit cell, Na is Avogadro's number, ρ is the density, M is the molar mass, h is Planck's constant, and k_B is Boltzmann's constant.

Table 5 summarizes the thermal and mechanical properties of SnAlSiH and SnGaSiH, computed using the GGA method under zero pressure conditions. The data show that SnAlSiH exhibits stronger atomic bonding than SnGaSiH, as indicated by its higher sound velocities ($v_t = 2469.34$ m/s, $v_l = 4861.74$ m/s, $v_m = 2767.53$ m/s) and higher Debye temperature ($\theta_D = 294.725$ K). In contrast, SnGaSiH has lower values ($v_t = 1992.52$ m/s, $v_l = 4077.66$ m/s, $v_m = 2238.17$ m/s, $\theta_D = 234.443$ K), reflecting weaker atomic bonds.

The inverse relationship between θ_D and molecular mass explains these differences, as SnGaSiH's larger mass results in a lower θ_D [52]. The agreement between θ_D values obtained from elastic constants (C_{ij}) and those predicted by thermodynamic models such as Gibbs2 reinforces the reliability of the computational approach.

These findings suggest that SnAlSiH, with its superior thermal conductivity and fracture resistance, is ideal for applications requiring mechanical and thermal stability, whereas SnGaSiH's greater thermal flexibility makes it better suited for environments with fluctuating stresses.

The mechanical behavior of materials—including asymmetric plastic deformation, fracture mechanisms, and structural instabilities—is profoundly governed by the elastic anisotropy of the crystal lattice [44]. For structural hydrides intended for hydrogen storage applications, a comprehensive understanding of this elastic heterogeneity is essential to predict performance and durability under cyclic loading and hydrogenation. A quantitative assessment of this anisotropy is achieved by calculating the anisotropic shear moduli, denoted as A_1 and A_2 for hexagonal systems. These coefficients directly quantify the disparity in bond stiffness across different crystallographic planes, providing critical insight into directional mechanical response. For hexagonal crystals, these coefficients are defined by the following relations [53]:

$$A_1 = 4C_{44} / \left(C_{11} + C_{33} - 2C_{13}\right) \tag{22}$$

$$A_2 = 2C_{66} / \left(C_{11} - C_{12}\right) \tag{23}$$

In this case, shear anisotropy is quantified in the {100} plane by A_1 and in the {001} plane by A_2. A_1 values for SnAlSiH and SnGaSiH are roughly 1.775 and 1.354, respectively, according to Table 5 (using the GGA approximation), while $A_2 = 1$ for both compounds. This shows noticeable anisotropy in the {100} plane but isotropic shear behavior in the {001} plane.

The relative anisotropy indices for bulk (A_B) and shear (A_G) moduli, which are computed as follows, are used for additional analysis [53]:

$$A_B = \left(B_V - B_R\right) / \left(B_V + B_R\right) \times 100 \tag{24}$$

$$A_G = \left(G_V - G_R\right) / \left(G_V + G_R\right) \times 100 \tag{25}$$

where G_V and G_R (Voigt and Reuss shear moduli) represent shear response variations, and B_V and B_R (Voigt and Reuss bulk moduli) evaluate volumetric compressibility heterogeneity. Table 5 shows that SnAlSiH has $A_B \approx 8.722\%$ and $A_G \approx 6.604\%$, while SnGaSiH has $A_B \approx 10.497\%$ and $A_G \approx 7.528\%$. Due of variations in the distribution of atomic bonds and microcrystalline structure, SnGaSiH exhibits a greater directional dependency on mechanical characteristics, which is highlighted by its larger anisotropy.

The universal elastic anisotropy index (A^U) offers a thorough evaluation., which is defined as [53]:

$$A^U = 5\frac{G_V}{G_R} + \frac{B_V}{B_R} - 6 \tag{26}$$

Perfect isotropy is represented by $A^U = 0$, and growing heterogeneity is shown by positive numbers. Table 5 confirms the increased elastic anisotropy of SnGaSiH by reporting $A^U \approx 1.0486$ and $A^U \approx 0.8982$ for SnAlSiH. The structural differences in the distribution of bulk and shear moduli, which are based on the distinct crystallographic characteristics of each compound, are the cause of this divergence [54]. In order to create innovative materials with customized mechanical performance for next-generation energy applications, these insights are essential.

Current studies on crystalline elastic properties lack sufficient depth to fully address directional anisotropies, limiting the understanding of material behavior under stress. To overcome this, integrating advanced metrics such as compliance-derived Young's modulus (E) and linear compressibility (B) is crucial, particularly for orientation-dependent or surface-sensitive systems.

Linear compressibility offers insights into anisotropic deformation patterns by quantifying dimensional changes under hydrostatic pressure along specific crystallographic axes. For hexagonal crystals, B is defined as:

$$B = \left(S_{11} + S_{12} + S_{13}\right) - n_2^3\left(S_{11} + S_{12} - S_{13} - S_{33}\right) \tag{27}$$

where the directional cosines (n_1, n_2, n_3) and elastic constants C_{ij} are correlated with the S_{ij} components of the compliance tensor.

In addition, orientation-dependent deformation is captured by Young's modulus compliance (E^{-1}), which is essential for forecasting directional stiffness. E is obtained for hexagonal lattices from [55]:

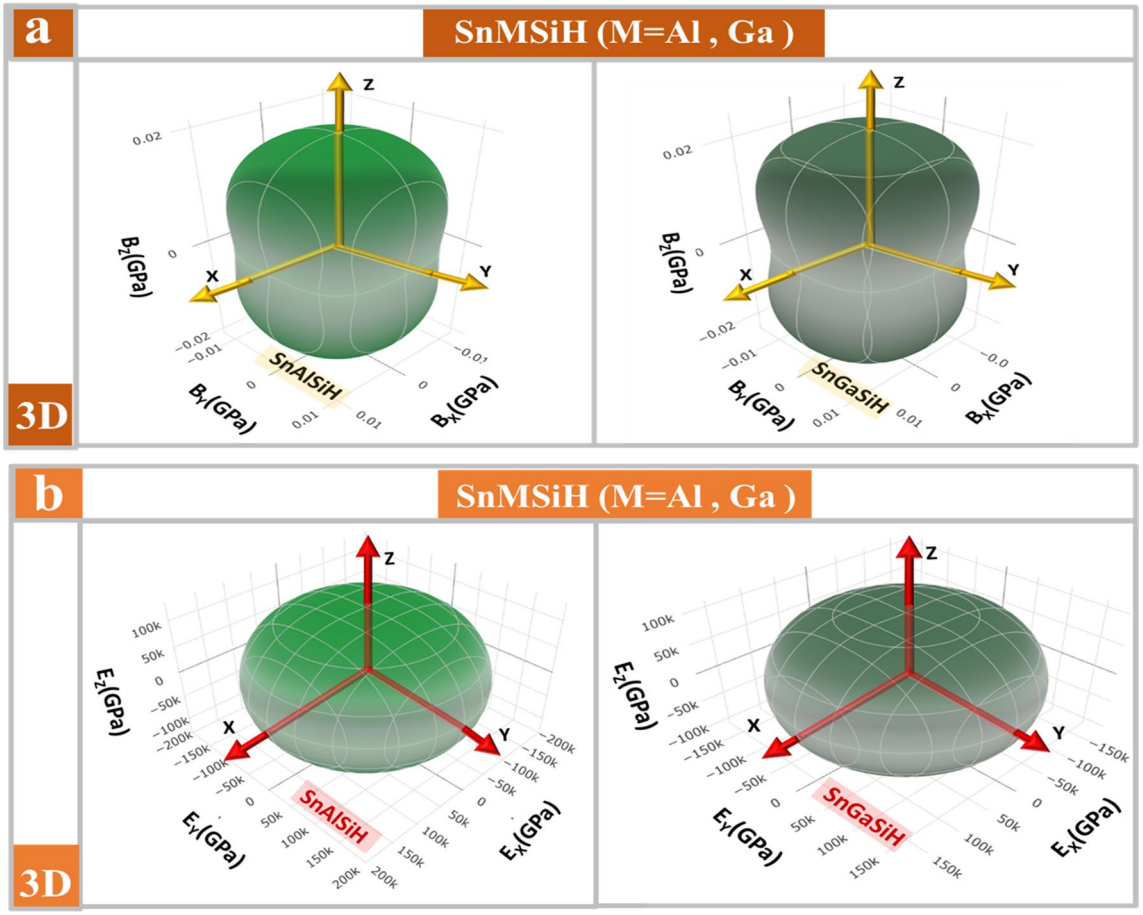

FIGURE 11 | (a) Three-dimensional representation of the Young's modulus distribution and (b) anisotropic linear compressibility for SnAlSiH and SnGaSiH compounds.

$$E^{-1} = \left(1-n_3^2\right)^2 S_{11} + n_3^4 S_{33} + n_3^2\left(1-n_3^2\right)\left(2S_{13}+S_{44}\right) \quad (28)$$

Hexagonal crystals exhibit significant anisotropy; for instance, compressibility along the *c*-axis ($n_3 = 1$) often differs substantially from responses in the basal plane ($n_3 = 0$), indicating variations in bond rigidity. Similarly, Young's modulus can differ by more than 50% along major crystallographic axes, necessitating a multidirectional assessment. By combining linear compressibility (B) and Young's modulus (E) with traditional bulk and shear moduli, a deeper insight into elastic properties can be achieved. This approach enables accurate predictions of fracture initiation, surface stability, and directional deformation, particularly in materials designed for hydrogen storage applications. As a result, these findings improve theoretical models and provide guidance for the design of mechanically resilient materials [54, 56].

The distributions of Young's modulus (Figure 11a) for SnAlSiH and SnGaSiH, derived from compliance constants, reveal that while these materials exhibit low elastic asymmetry, certain planes display moderate anisotropy. Specifically, the (XY) plane demonstrates isotropic stiffness, whereas the (X = Y), (XZ), and (YZ) planes show mild variations. The elastic constants C_{11}, C_{33}, and C_{44} further define the mechanical stability of these materials. Higher C_{11} and C_{33} values indicate greater resistance to lattice expansion, which is crucial for hydrogen absorption stability, while larger C_{44} values suggest stronger shear resistance during hydrogen desorption.

The elastic response of SnGaSiH and SnAlSiH is highly anisotropic, as evidenced by three-dimensional surface plots of linear compressibility (Figure 11b). This analysis reveals a significant orientation-dependence, where the (XY) basal plane exhibits markedly lower anisotropy between its in-plane axes compared with other crystallographic planes. This is characteristic of hexagonal lattices, where compressibility remains consistent within the basal plane but varies significantly out-of-plane, underscoring the necessity for a detailed elastic analysis.

These compounds exhibit rapid elastic recovery and positive elastic moduli across all directions, ensuring minimal hysteresis during pressure cycling—a critical trait for reversible hydrogen (de)sorption and long-term structural integrity. This resilience, combined with a high resistance to microcrack formation from cyclic expansion, directly enhances their durability. Furthermore, the mapping of Young's modulus provides invaluable insight for optimizing load-bearing orientations in device design, enabling the mitigation of stress concentrations and significantly improving resistance to hydrogen embrittlement and fatigue.

By strategically leveraging their combination of elastic recovery, directional stiffness, and tunable compressibility, SnMSiH materials can be engineered to maximize hydrogen absorption efficiency while robustly maintaining structural integrity over repeated cycles.

4 | Conclusion

This study presents the first in-depth investigation into the structural, electronic, thermodynamic, and mechanical properties of SnMSiH (M = Al, Ga) compounds, shedding light on their remarkable potential as advanced hydrogen storage materials. The compounds crystallize in a primitive hexagonal (P3m1) structure, a crucial feature that optimizes hydrogen absorption and release dynamics. The unique layered atomic arrangement of Ga, Si, and Al facilitates efficient hydrogen diffusion pathways, ensuring rapid and reversible hydrogen uptake—a key requirement for long-term, sustainable storage with minimal degradation.

The thermodynamic stability of SnMSiH compounds further underscores their suitability for real-world hydrogen storage applications. From an electronic perspective, their semi-metallic nature, devoid of substantial band gaps, enhances charge carrier mobility and fosters stronger hydrogen–metal interactions. The delocalization of electronic states lowers the activation energy for hydrogen desorption, thereby supporting efficient cycling performance. Additionally, the hybridization of orbitals near the Fermi level indicates a robust coupling between the electronic and lattice degrees of freedom, which may stabilize hydrogen within the material matrix. These insights suggest that the electronic properties of SnMSiH could be optimized through strategies like alloying or defect manipulation, further improving hydrogen absorption kinetics.

Thermodynamic analysis reveals significant thermal expansion, yet the compounds retain their structural integrity across a broad temperature range. Their strong vibrational stability, as indicated by calculated heat capacities and Debye temperatures, ensures reliable hydrogen storage even in fluctuating thermal environments. This resilience is invaluable in hydrogen storage applications, where temperature changes can disrupt the absorption–desorption equilibrium. Additionally, the moderate entropy change observed during hydrogen release suggests these materials can operate effectively in diverse environments, from ambient to elevated temperatures.

On the mechanical front, SnMSiH compounds display notable anisotropic behavior, particularly in shear modulus variations along different crystallographic planes. This anisotropy affects the material's mechanical response during hydrogen absorption and desorption cycles, where it must accommodate volumetric changes without structural failure. Among the compounds studied, SnAlSiH exhibits the highest compressibility, followed by SnGaSiH, indicating adequate mechanical flexibility for repeated hydrogenation cycles. Their high bulk modulus further confirms their mechanical stability, an essential feature for ensuring prolonged operational lifetimes in hydrogen storage applications.

In addition to their hydrogen storage capabilities, the interplay of electronic and mechanical properties in SnMSiH compounds opens the door to potential multifunctional applications. Their semi-metallic behavior, combined with structural robustness, makes them promising candidates for hybrid energy storage systems that integrate both hydrogen storage and electronic functionality. Furthermore, their mechanical resilience positions them as suitable candidates for flexible or lightweight hydrogen storage devices, where durability is paramount.

Future research should focus on strategies to enhance the hydrogen storage capacity of SnMSiH compounds. Techniques like doping with transition metals could fine-tune their electronic properties and improve hydrogen binding energies, while nanostructuring and composite material integration could further optimize hydrogen diffusion pathways. Exploring defect chemistry and phonon-lattice interactions may provide deeper insights into their hydrogen sorption mechanisms, paving the way for more efficient material designs. Moreover, employing advanced computational approaches, such as machine learning-assisted materials discovery, could accelerate the identification of modifications that improve hydrogen storage performance.

Overall, SnMSiH (M = Al, Ga) compounds stand out as highly promising candidates for advanced hydrogen storage applications, offering a perfect blend of structural stability, electronic conductivity, thermal resilience, and mechanical strength. Their capacity for efficient, reversible hydrogen absorption and release, coupled with inherent durability, positions them as strong contenders for sustainable energy storage solutions. Further computational and experimental research will be crucial in refining their properties and expediting their implementation in hydrogen-based energy systems.

Conflicts of Interest

The authors declare no conflicts of interest.

Data Availability Statement

The data that support the findings of this study are available from the corresponding author upon reasonable request.

References

1. M. J. B. Kabeyi and O. A. Olanrewaju, "Sustainable Energy Transition for Renewable and Low Carbon Grid Electricity Generation and Supply," *Frontiers in Energy Research* 9 (2022): 743114.

2. V. S. Arutyunov and G. V. Lisichkin, "Energy Resources of the 21st Century: Problems and Forecasts. Can Renewable Energy Sources Replace Fossil Fuels," *Russian Chemical Reviews* 86, no. 8 (2017): 777–804.

3. B. Harsanto, A. Mulyana, Y. A. Faisal, and V. M. Shandy, "Open Innovation for Sustainability in the Social Enterprises: An Empirical Evidence," *Journal of Open Innovation: Technology, Market, and Complexity* 8, no. 3 (2022): 160.

4. M. G. Rasul, M. A. Hazrat, M. A. Sattar, M. I. Jahirul, and M. J. Shearer, "The Future of Hydrogen: Challenges on Production, Storage and Applications," *Energy Conversion and Management* 272 (2022): 116326.

5. L. Cherwoo, I. Gupta, G. Flora, et al., "Biofuels an Alternative to Traditional Fossil Fuels: A Comprehensive Review," *Sustainable Energy Technologies and Assessments* 60 (2023): 103503.

6. L. Ge, B. Zhang, W. Huang, et al., "A Review of Hydrogen Generation, Storage, and Applications in Power System," *Journal of Energy Storage* 75 (2024): 109307.

7. T. Ghellab, Z. Charifi, H. Baaziz, et al., "Physical Properties of LiXH4 (X= B, Al) Hydrogen Storage Materials: Ab-Initio Study," *Solid State Communications* 347 (2022): 114731.

8. T. Saadi, H. Baaziz, T. Ghellab, H. Latelli, A. Telfah, and Z. Charifi, "Electronic Structure, Mechanical and Optical Properties of Hydrogen Storage Alkaline Amides XNH_2 (X= Li, Na) Compounds," *International Journal of Hydrogen Energy* 102 (2025): 1480–1496.

9. J. L. Holechek, H. M. E. Geli, M. N. Sawalhah, and R. Valdez, "A Global Assessment: Can Renewable Energy Replace Fossil Fuels by 2050?," *Sustainability* 14, no. 8 (2022): 4792.

10. S. G. Nnabuife, E. Oko, B. Kuang, et al., "The Prospects of Hydrogen in Achieving Net Zero Emissions by 2050: A Critical Review," *Sustainable Chemistry for Climate Action* 2 (2023): 100024.

11. L. Q. Chen and Y. Zhao, "From Classical Thermodynamics to Phase-Field Method," *Progress in Materials Science* 124 (2022): 100868.

12. P. Hoffmann, "Tomorrow's Energy: Hydrogen, Fuel Cells, and the Prospects for a Cleaner Planet," 2006.

13. S. Fang, J. Li, K. Zou, et al., "Zintl Chemistry: Current Status and Future Perspectives," *Chemical Engineering Journal* 433 (2022): 133841.

14. S. M. Kauzlarich, "Zintl Phases: From Curiosities to Impactful Materials," *Chemistry of Materials* 35, no. 18 (2023): 7355–7362.

15. M. Jamal, M. Bilal, I. Ahmad, and S. Jalali-Asadabadi, "IRelast Package," *Journal of Alloys and Compounds* 735 (2018): 569–579.

16. T. Bj¨orling, D. Nor'eus, K. Jansson, et al., "SrAlSiH: A Polyanionic Semiconductor Hydride," *Angewandte Chemie International Edition in English* 44, no. 44 (2005): 7269–7273.

17. J. A. Brehm, "Predicted Bulk Photovoltaic Effect in Hydrogenated Zintl Compounds," *Journal of Materials Chemistry C* 6, no. 6 (2018): 1470–1475.

18. M. H. Lee, T. Bj¨orling, B. C. Hauback, et al., "Crystal Structure, Electronic Structure, and Vibrational Properties of M AlSiH (M=Ca, Sr, Ba): Hydrogenation-Induced Semiconductors From the AlB 2-ty," 2008.

19. M. J. Evans, G. P. Holland, F. J. Garcia-Garcia, and U. H¨aussermann, "Polyanionic Gallium Hydrides From AlB2-Type Precursors AeGaE (Ae=ca, Sr, Ba; E=Si, Ge, Sn)," *Journal of the American Chemical Society* 130, no. 36 (2008): 12139–12147.

20. Y. Lu, T. Tada, Y. Toda, et al., "Interlayer States Arising From Anionic Electrons in the Honeycomb-Lattice-Based Compounds A e AlSi (A E=ca, Sr, Ba)," *Physical Review B: Condensed Matter* 95, no. 12 (2017): 125117.

21. V. F. Kranak, M. J. Evans, L. L. Daemen, et al., "Structural and Dynamic Properties of the Polyanionic Hydrides SrAlGeH and BaAlGeH," *Solid State Sciences* 11 (2009): 1847.

22. H. Ammi, Z. Charifi, H. Baaziz, T. Ghellab, L. Bouhdjer, and S. Adalla, "Electronic, Elastic, and Thermodynamic Properties of Complex Hydrides XAlSiH (X= Sr, ca, and Ba) Intended for Hydrogen Storage: An Ab-Initio Study," *Physica Scripta* 99, no. 6 (2024): 0659a2.

23. H. Ammi, Z. Charifi, H. Baaziz, et al., "Investigation on the Hydrogen Storage Properties, Electronic, Elastic, and Thermodynamic of Zintl Phase Hydrides XGaSiH (X= Sr, Ca, Ba)," *International Journal of Hydrogen Energy* 87 (2024): 966–984.

24. F. Tran, "WIEN2k: An Augmented Plane Wave Plus Local Orbitals Program for Calculating Crystal Properties," 2018.

25. J. P. Perdew, K. Burke, and M. Ernzerhof, "Generalized Gradient Approximation Made Simple," *Physical Review Letters* 77 (1996): 3865–3868.

26. A. Otero-de-la-Roza, D. Abbasi-P'erez, and V. Lua~na, "Gibbs2: A New Version of the Quasiharmonic Model Code. II. Models for Solid-State Thermodynamics, Features and Implementation," *Computer Physics Communications* 182 (2011): 2232.

27. A. Otero-de-la-Roza and V. Lua~na, "Gibbs2: A New Version of the Quasi-Harmonic Model Code. I. Robust Treatment of the Static Data," *Computer Physics Communications* 182 (2011): 1708.

28. M. A. Blanco, E. Francisco, and V. Lua~na, "GIBBS: Isothermal-Isobaric Thermodynamics of Solids from Energy Curves Using a Quasi-Harmonic Debye Model," *Computer Physics Communications* 158 (2004): 57.

29. L. A. Girifalco, *Interfacial Science: An Introduction* (Oxford University Press, 2000).

30. S. Guatelli, A. Mantero, B. Mascialino, P. Nieminen, and M. G. Pia, "Geant4 Atomic Relaxation," *IEEE Transactions on Nuclear Science* 54, no. 3 (2007): 585–593.

31. V. G. Tyuterev and N. Vast, "Murnaghan's Equation of State for the Electronic Ground State Energy," *Computational Materials Science* 38, no. 2 (2006): 350–353.

32. S. Al, C. Kurkcu, and C. Yamcicier, "Structural Evolution, Mechanical, Electronic and Vibrational Properties of High Capacity Hydrogen Storage TiH4," *International Journal of Hydrogen Energy* 45, no. 55 (2020): 30783–30791.

33. K. Archana, N. G. Pillai, K. V. Sai Srinivasan, et al., "Enhanced Isosteric Heat of Adsorption and Gravimetric Storage Density of Hydrogen in GNP Incorporated Cu Based Core-Shell Metal-Organic Framework," *International Journal of Hydrogen Energy* 45, no. 58 (2020): 33818–33831.

34. P. M. Mathias, "The Gibbs–Helmholtz Equation in Chemical Process Technology," *Industrial & Engineering Chemistry Research* 55, no. 4 (2016): 1076–1087.

35. V. Berube, G. Chen, and M. S. Dresselhaus, "Impact of Nanostructuring on the Enthalpy of Formation of Metal Hydrides," *International Journal of Hydrogen Energy* 33, no. 15 (2008): 4122–4131.

36. L. K. Bhaskar, N. Moharana, H. Holz, R. Ramachandramoorthy, K. C. H. Kumar, and R. Kumar, "Probing Elastic Isotropy in Entropy Stabilized Transition Metal Oxides: Experimental Estimation of Single Crystal Elastic Constants From Polycrystalline Materials," *Acta Materialia* 288 (2025): 120871.

37. F. Mouhat and F. X. Coudert, "Necessary and Sufficient Elastic Stability Conditions in Various Crystal Systems," *Physical Review B: Condensed Matter* 90, no. 22 (2014): 224104.

38. N. Erum and M. A. Iqbal, "Ab Initio Study of High Dielectric Constant Oxide-Perovskites: Perspective for Miniaturization Technology," *Materials Research Express* 4, no. 2 (2017): 025904.

39. T. Ghellab, Z. Charifi, H. Baaziz, et al., "The Elastic, Mechanical, and Thermodynamic Properties of NaXH4 (X=B, Al) Intended for the Storage of Hydrogen: An Ab-Initio Study," *Physica B: Condensed Matter* 638 (2022): 413851.

40. R. Hill, "The Elastic Behaviour of a Crystalline Aggregate," *Proceedings of the Physical Society. Section A* 65, no. 5 (1952): 349–354.

41. R. Hill, "New Derivation of Some Elastic Extremum Principles," Progress in Applied Mechanics, The Prager Anniversary 1963;Ume:99–106.

42. W. Voigt, *Lehrbuch Der Kristallphysik (Textbook of Crystal Physics)* (BG Teubner, 1928).

43. A. Reuss, "Calculation of the Flow Limits of Mixed Crystals on the Basis of the Plasticity of Monocrystals," *Zeitschrift für Angewandte Mathematik Und Mechanik* 9, no. 1 (1929): 49–58.

44. D. R. França and A. Blouin, "All-Optical Measurement of In-Plane and Out-Of-Plane Young's Modulus and Poisson's Ratio in Silicon Wafers by Means of Vibration Modes," *Measurement Science and Technology* 15, no. 5 (2004): 859–868.

45. R. Caputo and A. Tekin, "Ab-Initio Crystal Structure Prediction. A Case Study: NaBH4," *Journal of Solid State Chemistry* 184, no. 7 (2011): 1622–1630.

46. J. M. Wills, O. Eriksson, P. S¨oderlind, and A. M. Boring, "Trends of the Elastic Constants of Cubic Transition Metals," *Physical Review Letters* 68, no. 18 (1992): 2802.

47. M. Nakamura, *Intermetallic Compounds: Principles*, vol. 1, ed. J. H. Westbrook and R. L. Fleischer (Wiley, 1994), 873.

48. S. F. Pugh, "XCII. Relations Between the Elastic Moduli and the Plastic Properties of Polycrystalline Pure Metals," *London, Edinburgh, and Dublin Philosophical Magazine and Journal of Science* 45, no. 367 (1954): 823–843.

49. N. A. A. Rusman and M. Dahari, "A Review on the Current Progress of Metal Hydrides Material for Solid-State Hydrogen Storage Applications," *International Journal of Hydrogen Energy* 41, no. 28 (2016): 12108–12126.

50. O. L. Anderson, "A Simplified Method for Calculating the Debye Temperature From Elastic Constants," *Journal of Physics and Chemistry of Solids* 24, no. 7 (1963): 909–917.

51. K. J. Gross, G. J. Thomas, and C. M. Jensen, "Catalyzed Alanates for Hydrogen Storage," *Journal of Alloys and Compounds* 330 (2002): 683–690.

52. S. Y. Davydov and O. V. Posrednik, "On the Theory of Elastic Properties of Two-Dimensional Hexagonal Structures," *Physics of the Solid State* 57 (2015): 837–843.

53. K. B. Panda and K. R. Chandran, "Determination of Elastic Constants of Titanium Diboride (TiB2) From First Principles Using FLAPW Implementation of the Density Functional Theory," *Computational Materials Science* 35, no. 2 (2006): 134–150.

54. S. I. Ranganathan and M. Ostoja-Starzewski, "Universal Elastic Anisotropy Index," *Physical Review Letters* 101, no. 5 (2008): 055504.

55. J. F. Nye, *Physical Properties of Crystals: Their Representation by Tensors and Matrices* (Oxford university press, 1985).

56. R. F. S. Hearmon, "The Elastic Constants of Anisotropic Materials—II," *Advances in Physics* 5, no. 19 (1956): 323–382.